LIP-STUDENTS-19-06

Search for exclusive top quark pair production at the LHC

Miguel Nobre Guerreiro[1,a]

[1] *Instituto Superior Técnico, Lisboa, Portugal*

Project supervisors: M. Gallinaro, B. Lopes

October 2019

Abstract. As the heaviest particle in Standard Model, top quark is one of the current focuses of the LHC programme to search for new physics. This internship focused on the search for exclusively produced top quark pairs in the CMS experiment. In this project I performed a kinematic analysis of Monte Carlo samples of events in proton-proton collisions at a center-of-mass (CM) energy of 13 TeV, using information from the CMS central detector and the Precision Proton Spectrometer (PPS). By comparing the normalized distributions of exclusive $t\bar{t}$, inclusive $t\bar{t}$ and Drell-Yan regarding different kinematic variables, I could identify the ones that best discriminate signal from background and the respective selection cuts to apply. With this work, I was able to set the basis for a multivariate analysis that could be used on real data, through machine learning techniques.

KEYWORDS: CMS, PPS, $t\bar{t}$, exclusive production, Monte Carlo, kinematic analysis

1 Introduction

1.1 Standard model and top quark

The Standard Model (SM) of particle physics is a theory which encloses all known fundamental particles and a description for the electromagnetic, strong and weak interactions that govern them. Developed in the early 1970s, it is considered a well-tested physics theory, in the sense that it has explained almost all collider experimental results and precisely predicted a wide variety of phenomena. Nevertheless, the SM displays some known limitations: on one hand, it only offers a description for three of the four interactions in the Universe (not accounting for gravitational force), and does not foresee a suitable candidate for dark matter; on the other hand, the CP violation described by the SM may be insufficient to account for the matter-antimatter asymmetry of the Universe. So, although the SM accurately describes phenomena within its domain, it is not seen as the complete picture, which thus motivates experimental searches for Beyond the Standard Model (BSM) physics [1].

Top quark is the heaviest particle described by the SM and it was discovered in 1995 [2]. Because of its large mass, it is a fundamental particle of special interest for being potentially more sensitive to SM deviations. Top quark is produced at the LHC mainly in the form of $t\bar{t}$ pairs and decays almost exclusively in the SM to a b quark and a W boson [3]. The b quark will hadronize, producing a jet (b-jet). Therefore, the final products of a $t\bar{t}$ decay depend on the W boson decays, which can be through three possible channels: *all-jets* (when both W bosons decay to $q\bar{q}$ pairs which then hadronize), *lepton+jets* (when one W decays to a $q\bar{q}$ pair and the other to a lepton and the corresponding neutrino), and *dileptons* (when both W bosons decay each into a lepton and the corresponding neutrino). The dileptonic decaying channel was the one I focused on for this exclusive $t\bar{t}$ production search, as it offers a higher purity. Moreover, there is a better detection capability for leptons with respect to jets, caused by the superior efficiency of trackers over calorimeters in CMS, which will be addressed in the following section.

1.2 Exclusive $t\bar{t}$ production

In a proton-proton collision, some of the quarks and gluons from one of the protons will interact with those from the other proton at high-energy, resulting, in general, in the disruption of the initial protons. In some collisions, however, these protons may interact by exchanging energetic photons, which combine producing new particles, while either one or both initial protons are kept intact, as shown in figure 1. These are called exclusive processes (or semi-exclusive, for when only one proton remains intact) [4]. This kind of process is rare but extremely interesting when the detection of the interacting protons is possible through forward detectors, which is the case at the CMS experiment, with the Proton Precision Spectrometer (PPS) described in the next section. The detection of the escaping protons allows the determination of their energy loss in the interaction. Thus, it makes possible the kinematic reconstruction of the system, despite the existence of Missing Transverse Energy (MET) due to the neutrinos in the W boson decays in the dilepton decay channel, which cannot be detected.

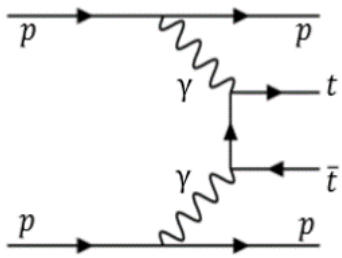

Figure 1. Exclusive $t\bar{t}$ production diagram, via $\gamma\gamma$ fusion.

[a] e-mail: miguel.nobre.guerreiro@tecnico.ulisboa.pt

1.3 Main background

In order to identify the final products of the exclusive $t\bar{t}$ process in the central detector, we applied the central selection described on the next section, which results in two main types of background: Drell-Yan and inclusive $t\bar{t}$.

1.3.1 Drell-Yan

The Drell-Yan (DY) process is an electromagnetic effect in which a quark and an antiquark from the pair of scattered protons interact by annihilation, creating a virtual photon or a Z boson which then decay to give a lepton pair. The representative diagram is shown in figure 2. This process constitutes a background in our analysis since it has two leptons as final products. Besides, the interacting quarks can sometimes emit gluons, which will then decay into a new quark-antiquark pair that will hadronize and originate a jet.

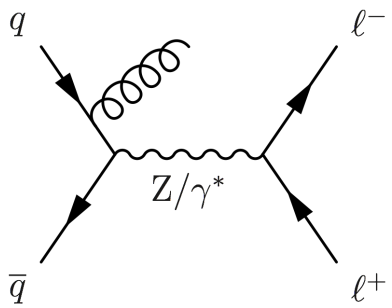

Figure 2. Drell-Yan process representative diagram.

1.3.2 Inclusive $t\bar{t}$

Accounting for the explanation given in the previous subsection, inclusive $t\bar{t}$ events include all the processes resulting in a top quark pair in which the initial protons are disrupted. In this case, the protons interact not by electroweak force (as it happens on the exclusive $t\bar{t}$ process, mediated through photon-photon interactions), but by fusion of gluons - mediated by the strong interaction. This process, represented in figure 3, possesses a totally identical central detector signature when compared to exclusive $t\bar{t}$ and, therefore, is the hardest background to discriminate from signal.

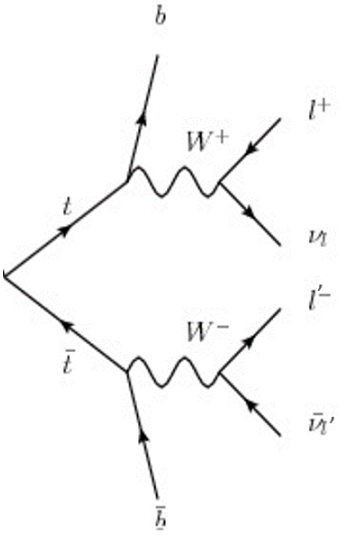

Figure 3. Inclusive $t\bar{t}$ process diagram, representative of the dilepton final state.

2 Methodology

2.1 Compact Muon Solenoid (CMS)

The CMS (Compact Muon Solenoid) detector is one of the detectors at the LHC. It has a cylindrical shape and, as depicted in figure 4, consists on a central region where the collisions occur, followed by a silicon tracker which tracks the passage of charged particles (which curve in opposite directions for particles with opposite charge), then an electromagnetic calorimeter, where photons and electrons typically deposit their energy in the form of energy clusters (showers), and an hadronic calorimeter, where hadrons deposit their energy. Continuing outwards, there is the superconducting solenoid which produces the 3.8 T magnetic field and the muon chambers, with up to four stations of gas-ionization muon detectors installed outside the solenoid and sandwiched between the layers of the steel return yoke. (A full description can be found in [5]).

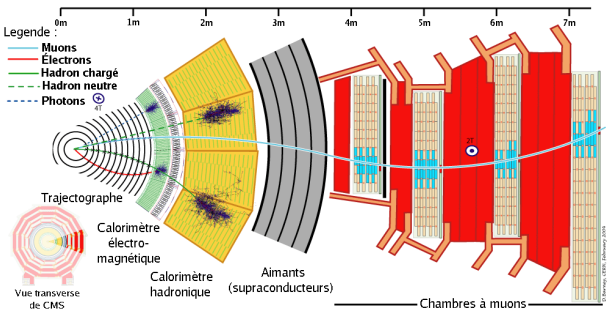

Figure 4. Schematic transverse view of a slice of the CMS detector.

2.2 Precision Proton Spectrometer (PPS)

The PPS (Precision Proton Spectrometer) [6] detector is the forward detector of CMS, approximately 200 m of

the interaction point (IP), and has the capacity to detect the scattered protons which suffered a momentum loss between 2 and 16%. It is composed of two sets of detectors (one on each side of the IP), called Roman Pots (RPs). These are movable devices, placed a few mm from the beamline, as represented in figure 5. The force suffered by a charged particle in the presence of a magnetic field is proportional to its velocity, as given by the simplification of the Lorentz formula:

$$\vec{F} = q \cdot (\vec{v} \times \vec{B}) \tag{1}$$

The external product between velocity and magnetic field vectors (with the latter pointing up when the velocity points forward - into the plane of the paper- and down when the velocity points backwards - out of the plane of the paper) in the second term of equation 1 originates a vector force pointing in the direction of the center of the detector - centripetal force, which formula is given by equation 2:

$$F = \frac{m \cdot v^2}{r} \tag{2}$$

Substituting equation 2 in equation 1, we can isolate the radius to obtain the following relation:

$$r = \frac{mv}{qB} \tag{3}$$

Meaning that a decrease in the particle velocity implies a decrease in the gyro-radius. According to this relation, the LHC magnets are built to create a magnetic field with specific intensities, so to apply the right force over the circulating protons (with initial energies - and thus velocities - preserved), in order to bend them according to the specific radius that keeps them inside the beam line. Therefore, by losing momentum during the interaction, the scattered protons decrease the radius of their trajectory and will eventually get out of the beam envelope, allowing the strategically positioned RP to detect them with a given acceptance. For a momentum loss of 2 to 16 percent, the protons are expected to get out of the beam envelope at about 200 m of the IP and arrive within the PPS detector acceptance.

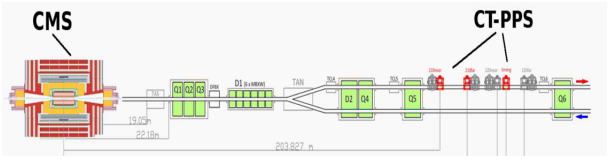

Figure 5. A schematic view of the PPS right arm.

2.2.1 Forward tracks in PPS and pile-up

The importance of detecting the scattered protons lies on the ability to measure their momentum loss, reconstruct their kinematics and, finally, compare these measurements to the central detector kinematics, with the goal of finding correlations. With that in mind, the fractional momentum loss of each tracked proton in the RP is obtained through equation 4:

$$\xi = \frac{p_i - p_f}{p_i} \tag{4}$$

where p_i and p_f are the initial and final proton momenta. Since our process is exclusive, the objective is to detect two corresponding intact protons (in the RPs on opposite arms of the CMS central detector). Therefore, thanks to PPS, the reconstruction of tracks on both sides of the IP can be accomplished and the respective proton momentum losses can be calculated (ξ_1, ξ_2) [7]. By doing this, the mass and the rapidity of the system can be reconstructed for every possible combination of PPS-tracked protons using equations 5 and 6, respectively.

$$m_{RP} = \sqrt{s\xi_1\xi_2} \tag{5}$$

$$y_{RP} = \frac{1}{2} \ln\left(\frac{\xi_1}{\xi_2}\right) \tag{6}$$

Due to the high luminosity of the LHC bunch collisions, there is often more than one tracked proton in a RP, as discussed in subsection 3.2. This is caused by pile-up protons, or just because the vacuum in the LHC is not ideal and, thus, a proton can sometimes collide with some molecules (such as Oxygen) along its trajectory, and lose the required momentum to enter in the RP acceptance interval, resulting in random background. So, to determine the right combination of tracks that reconstructs our exclusive process, we require the reconstructed mass (m_{RP}) to be in between 300 and 600 GeV, since this is the range where we expect the bulk of signal production [7]. This selection removes most of the pile-up since there are events from 300 to 3000 GeV, but there is still a large amount of pile-up in this region. The solution lies in implementing a statistical study of the pile-up distribution that allows its estimation in order to look for an excess in data with respect to the prediction.

2.3 Central Selection

Bearing in mind the final products of the exclusive $t\bar{t}$ decay - described in the first section, and the work developed in [7], we applied a central selection requiring at least 2 leptons in the final state, with an absolute value of pseudo-rapidity inferior or equal to 2.5, and a minimum transverse momentum of 13 GeV. It was also required at least 1 jet, and at least 1 b-jet in the analysis.

3 Results and Discussion

In order to learn how to better differentiate signal from background, we performed a kinematic analysis on simulated samples, with a CM total energy of 13 Tev, providing exclusive $t\bar{t}$ and the respective two main types of background (inclusive $t\bar{t}$ and DY) discriminated *à priori*. The samples include approximate simulation of the CMS and PPS detectors. The results shown are indicative and

represent a preliminary exploratory study. Two types of results were obtained: first, considering only the central detector, comparing signal and background regarding different kinematic variables and analyzing their distributions in normalized plots for selection of possible cuts. Second, using the simulated information of PPS for signal only, reconstructing the kinematics of the system and comparing it with the central detector, in the search for correlations.

3.1 Central Detector

3.1.1 Number of jets

Considering the jet multiplicity for the three processes, represented in figure 6, it is possible to observe that the inclusive $t\bar{t}$ distribution has a higher number of jets when compared to the distribution of exclusive $t\bar{t}$ events. This can be explained by the differences between the two processes in the production of $t\bar{t}$, already mentioned in the previous sections: exclusive $t\bar{t}$ results from a photon-photon interaction between the initial protons, mediated by electro-weak force; on the other hand, inclusive $t\bar{t}$ production is mediated by strong interaction, through the fusion of gluons from the two protons, which generates a higher number of quarks and gluons in the medium that will then hadronize, resulting in a higher number of jets.

For this variable, requiring a maximum jet multiplicity of 4 would remove background (inclusive $t\bar{t}$) without losing too much signal, thus increasing the significance of the analysis.

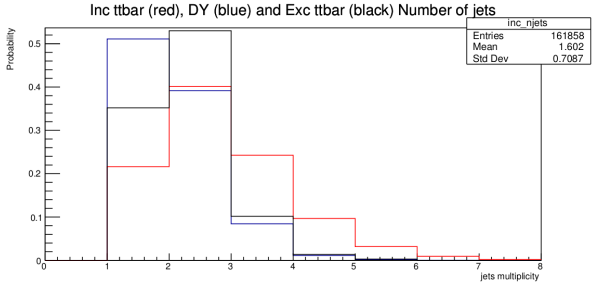

Figure 6. Number of jets for signal and background events. Distributions are normalized to unity.

3.1.2 Lepton-lepton invariant mass

Regarding the reconstructed mass of the two final leptons for each process, we found the results shown in figure 7. For DY, it was obtained the expected peak for a dilepton invariant mass at approximately 91.2 GeV - i.e. mass of the Z boson that decays into two oppositely charged leptons. On the other hand, for exclusive and inclusive $t\bar{t}$ events, the distribution does not peak at any particular value. This result is as expected since - in the case of $t\bar{t}$ events- the two leptons from the two W boson leptonic decays have uncorrelated momenta and their invariant mass does not peak at a particular value. We can also note in figure 7 that the dilepton invariant mass for the exclusive $t\bar{t}$ events is slightly more distributed to right (to higher energy values), which is expected since the two leptons of the exclusive $t\bar{t}$ are more energetic than the ones from the inclusive process.

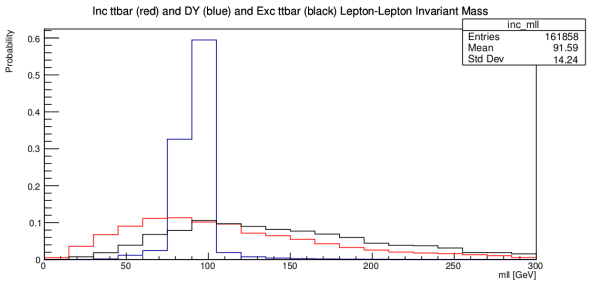

Figure 7. Dilepton invariant mass for signal and background events. Distributions are normalized to unity.

3.1.3 MET (Missing Transverse Energy)

Represented in figure 8 is the MET for the three processes. As expected, exclusive $t\bar{t}$ and inclusive $t\bar{t}$ have similar MET distributions, with a mean in the energy interval between 40 and 70 GeV. For DY, the MET has a lower mean (around 35 GeV). Although the DY decay channel in most cases does not have neutrinos, there is the case when the two final leptons are taus, which may decay leptonically, to electrons and muons and corresponding neutrinos (e.g. $\tau \rightarrow \ell\nu_\ell\nu_\tau$, where $\ell = e, \mu$). This can help to explain the MET observed in the DY process.

For this variable, a minimum MET requirement of 20 GeV would remove some DY from the analysis without losing too much signal.

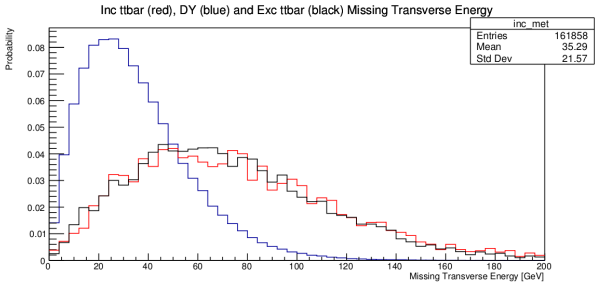

Figure 8. MET distribution for signal and background events. Distributions are normalized to unity.

3.1.4 Lepton-lepton $\Delta\phi$

Considering the leptonic $\Delta\phi$ (azimuthal angle between the two final leptons in the transverse plane) for the three processes, the result obtained is represented in figure 9. It is possible to observe a clear difference between signal and background, with the exclusive $t\bar{t}$ clearly distributed to higher values of delta phi when compared with the other two distributions. This result was expected since the two leptons of the exclusive process are more energetic and,

therefore, are more opposite to one another in the transverse plane.

This is the central detector kinematic variable that better discriminates exclusive $t\bar{t}$ from inclusive $t\bar{t}$ in this analysis. Therefore, requiring a minimum $\Delta\phi$ of 2 rad would remove background and thus increase the significance of the study.

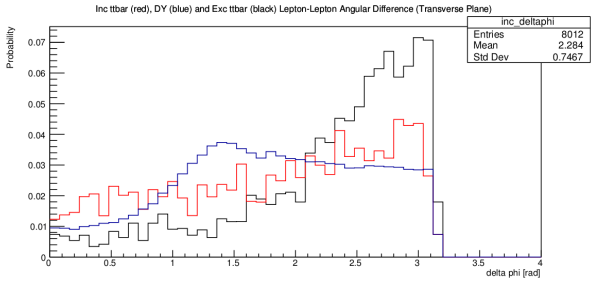

Figure 9. $\Delta\phi$ distribution between the two leptons, for signal and background events. Distributions are normalized to unity.

3.2 PPS - Roman Pots (RP)

3.2.1 Number of protons

In figure 10 is represented the distribution of the proton multiplicity for the RP stations on opposite sides of the interaction point (IP). As it is possible to observe, there is a considerable amount of events for which the number of detected protons is higher than 1. The higher proton multiplicity comes from pile-up, as discussed in section 2.2.1. For each detected proton we evaluate the respective fractional momentum loss (ξ).

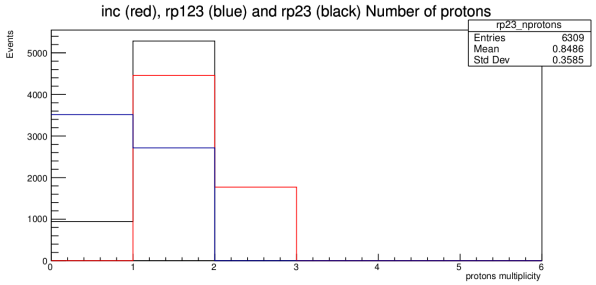

Figure 10. Number of protons for each event traversing the RP stations on opposite sides of the interaction point (black and blue), and their combination (red).

3.2.2 Fractional momentum loss (ξ)

Considering the ξ distribution of the protons detected in each RP, represented in figure 11, it is possible to conclude that the two PPS arms have a similar acceptance. A larger number of protons is at low values of ξ. However, in that region we are also dominated by random background, due to the superimposition of protons from beam-halo with inclusive $t\bar{t}$ events. Therefore, there are statistical approaches that can be applied to predict the probability of false RP proton detection, and then apply the respective correction factor when dealing with real data. From the ξ distribution, we calculate the mass (m_{RP}) and rapidity (y_{RP}) for each proton (from equations 5 and 6, respectively) and select the best combination of tracked protons for each event by applying the selection explained in the end of section 2.2.1. Afterwards, we correlate the kinematics of the selected duo of tracked protons with the kinematics of the central detector.

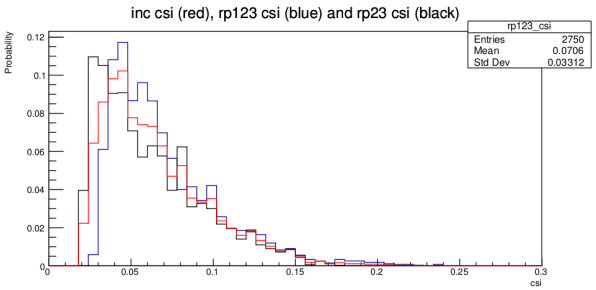

Figure 11. Distribution of the fractional momentum loss ξ for each proton arriving in the left (black) and in the right (blue) RP, and their combination (red). Distributions are normalized to unity.

3.2.3 Mass correlations

The correlation between the reconstructed mass of the interacting protons (m_{RP}) and the mass of the two final leptons from the respective $t\bar{t}$ decay ($m_{\ell\ell}$) is shown in the left plot of figure 12. For a true correlation between the two variable, there should be an accumulation of points along the diagonal. However, the points are scattered around, and not necessarily accumulated along the diagonal. This comes from the fact that the dilepton invariant mass is only an approximation of the energy of the $t\bar{t}$ decay. Therefore, we tried to perform a better approximation of the total energy deposited in the central detector by adding the reconstructed mass of b-jets to the mass of the two leptons, creating the variable m_{Vis}, which is the visible mass. The comparison between m_{Vis} and m_{RP} is represented by the right plot in figure 12. Although it is possible to observe an increased accumulation of points along the diagonal line, this correlation is not yet satisfactory, that can be explained by the MET which is due to the neutrinos that are to be accounted for. In order to obtain a better correlation with the reconstructed mass, an algorithm that performs an approximation of MET for each event could be applied.

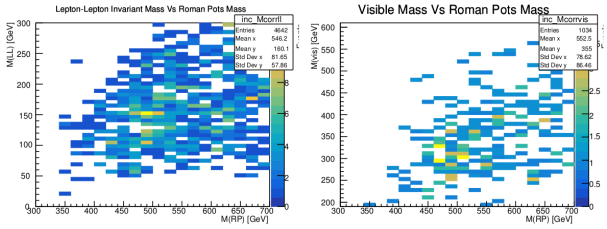

Figure 12. Left: Dilepton invariant mass ($m_{\ell\ell}$) as a function of the RP mass (m_{RP}). Right: visible mass (m_{Vis}) as a function of the the RP mass (m_{RP}).

3.2.4 Rapidity correlations

For rapidity and visible rapidity the correlations obtained between PPS and central detector are presented in figure 13 (left and right plots, respectively) and constitute more satisfactory results, indicated by the greater accumulation of points along the diagonal. The existence of this correlation is important and presents one more tool to search for exclusive top quark production when analyzing real data.

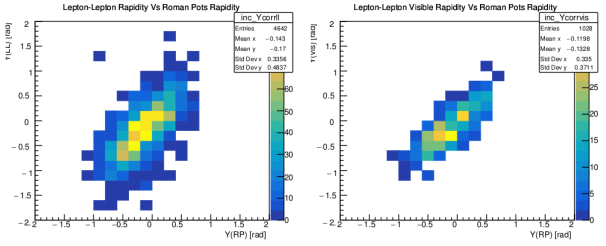

Figure 13. Left: Rapidity of the dilepton system ($y_{\ell\ell}$) as a function of the rapidity of the system of the two leading protons in the RPs (y_{RP}); Right: rapidity of the visible system (see text, y_{Vis}) as a function of y_{RP}.

4 Skills acquired

Over the course of this internship there were many skills I had the opportunity to develop: learned ROOT, matured my overall programming skills by learning C++, understood the basis of a physics analysis and expanded my knowledge on particle physics, LHC detectors and the day-to-day activity of a research institute such as LIP.

5 Conclusions

By analyzing the kinematical properties of the signal and background distributions in normalized plots, we could identify the most discriminatory ones, select the respective cuts to apply, and provide a physical explanation for the distributions obtained. Besides, we were able to find correlations between the reconstructed rapidity of the protons detected in the RPs of the PPS and the rapidity from the central detector particles for signal simulation. The correlations between PPS and central detector kinematics would be enhanced through the implementation of two algorithms: one to apply a correction factor on PPS in order to reduce pile-up, by predicting its frequency in the data through statistical studies on MC samples; and a second one to estimate the MET in each event by analyzing the kinematic parameters of the decaying process, and taking it into account in the calculations.

All these results are valid and could be implemented with a machine learning technique such as BDT, in order to enhance the detection of exclusive $t\bar{t}$ when working with real data.

Acknowledgements

I would like to thank every professor and investigator from LIP for being so devotedly involved in these summer internships. Particularly to Michele, and all the CMS group, for their availability to clear doubts and answer general questions; and to Nuno, for the commitment and enjoyment exhibited during the introductory week, every seminar that occurred, and the final workshops.

I would also like to thank the Master and PhD students for being so welcoming and predisposed to help, even with their thesis deadline coming up.

Especially, I want to thank Beatriz for her genuine interest in physics and in the process of teaching it, that greatly inspired me during these two months to absorb the maximum knowledge in every possible situation and reminded me of the importance of taking pleasure from learning.

References

[1] M. Thomson et al. (2018), modern Particle Physics. 1st ed

[2] F. Abe et al. (CDF), Phys. Rev. Lett. **74**, 2626 (1995), hep-ex/9503002

[3] M. Tanabashi et al. (2018), review of Particle Physics. Phys. Rev. D, 98(3):030001

[4] A.M. Sirunyan et al. (CMS, TOTEM), JHEP **07**, 153 (2018), 1803.04496

[5] CMS, JINST 3 (2008)

[6] M. Albrow et al. (CMS, TOTEM) (2014), precision Proton Spectrometer

[7] B. Lopes et al. (CMS, TOTEM) (2018), internal CMS analysis note AN-18-239